Check for updates

Photochemistry of P,N-bidentate rhenium(I) tricarbonyl complexes: reactive species generation and potential application for antibacterial photodynamic therapy†

Alison Acosta,[a] Javier Antipán,[b] Mariano Fernández,[b] Gaspar Prado,[b] Catalina Sandoval-Altamirano,[c] Germán Günther,[d] Izabook Gutiérrez-Urrutia,[e] Ignacio Poblete-Castro,‡[e] Andrés Vega [ID] *[b] and Nancy Pizarro [ID] *[b]

In this work, we describe the photoisomerization of facial rhenium(I) tricarbonyl complexes bearing P,N-bidentate pyridyl/phosphine ligands with different chelating rings and anions: **RePNBr**, **RePNTfO**, and **RePNNBr**, which are triggered under irradiation at 365 nm in solutions. The apparent photodegradation rate constants (k_{app}) depend on the coordinating ability of the solvent, being lowest in acetonitrile. The k_{app} value increases as the temperature rises, suggesting a reactive IL excited state thermally populated from the MLCT excited state involved. Using the Eyring equation, positive activation enthalpies ($\Delta H^{\neq}$) accompanied by high negative values for the activation entropy ($\Delta S^{\neq}$) were obtained. These results suggest whatever the P,N-ligand or anion, the reaction proceeds through a strongly solvated or a compact transition state, which is compatible with an associative mechanism for the photoisomerization. A 100-fold decrease in the $\log_{10}$ CFU value is observed for *E. coli* and *S. aureus* in irradiated solutions of the compounds, which follows the same tendency as their singlet oxygen generation quantum yield: **RePNBr** > **RePNTfO** > **RePNNBr**, while no antibacterial activity is observed in the darkness. This result indicates that the generation of singlet oxygen plays a key role in the antibacterial capacity of these complexes.

Introduction

Rhenium(I) tricarbonyl diimines are attractive compounds due to their unique luminescence properties.[1,2] They are easy to prepare, very stable at room temperature, and capable of emitting light in the visible region, and their photophysical properties are modulated by the ligands used.[3,4] Owing to these advantages, they have been used in a wide range of applications as follows: as photocatalysts for CO_2 reduction,[5–7] as biomolecular probes for sensing different microenvironments,[8,9] as DNA or protein probes for biolabeling,[10,11] as sensitizers for Grätzel-type solar cells,[12,13] and as singlet oxygen sensitizers for photodynamic therapy (PDT),[14] among others.

It is now very well established that excitation with UV-Vis light of Re^I–diimine complexes, $[(N,N)Re(CO)_3X]$ where X corresponds to a halide, mainly yields a triplet metal-to-ligand charge transfer (^{3}MLCT) excited state.[15–17] This is due to the extremely fast intersystem crossing process from the singlet to the triplet state, taking place normally in a few hundred femtoseconds and having a quantum yield close to unity.[18,19] Then, the ^{3}MLCT-excited state decays to the ground state by radiative and/or non-radiative processes or evolves to a photochemical path to yield products. Additionally, when molecular oxygen is present, energy transfer from ^{3}MLCT to oxygen may occur, generating singlet oxygen, $O_2(^1\Delta_g)$.[20–22]

The photochemistry of Re^I–diimine complexes has been less explored than their photophysical properties. Sato *et al.* reported that the facial isomer of $[(bpy)Re(CO)_3Cl]$ could be easily photo-converted into the meridional one under irradiation at 313 nm in a tetrahydrofuran solution.[23] Despite their structural similarities, the photophysical properties of the *fac* and *mer*-isomers and their reactivities are different (Scheme 1). Sato and co-workers also demonstrated that *fac*-[(bpy)Re(CO)_3Cl] (bpy = 2,2'-bipyridine)

[a]Universidad Técnica Federico Santa María, Centro de Biotecnología, Avenida España 1680, Valparaíso, Chile

[b]Universidad Andres Bello, Facultad de Ciencias Exactas, Departamento de Ciencias Químicas, Viña del Mar, Chile. E-mail: npizarro@unab.cl; andresvega@unab.cl

[c]Universidad de Santiago de Chile (USACH), Facultad de Química y Biología, Departamento de Ciencias del Ambiente, Chile

[d]Universidad de Chile, Facultad de Ciencias Químicas y Farmacéuticas, Departamento de Química Orgánica y Fisicoquímica, Santiago, Chile

[e]Universidad Andrés Bello, Facultad de Ciencias de la Vida, Center for Bioinformatics and Integrative Biology (CBIB), Biosystems Engineering Laboratory, Santiago, Chile

† Electronic supplementary information (ESI) available. See DOI: 10.1039/d1ra06416a

‡ Current address: Biosystems Engineering Laboratory, Department of Chemical Engineering, Universidad de Santiago de Chile (USACH), Chile.
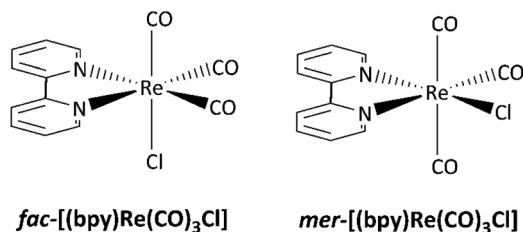
**Scheme 1** Facial and meridional isomers of [(bpy)Re(CO)₃Cl].[23]

undergoes a photoinduced carbonyl substitution after excitation at 313 nm in an acetonitrile solution, yielding two isomers.[24] The same photoreaction carried out in a constrained medium like a metal–organic framework (MOF) allows identifying the reactive intermediates, establishing a mechanism involving the release of one carbon monoxide molecule, CO.[25]

However, while the halide ligand can be thermally replaced with other ligands (such as pyridine, monodentate phosphorus ligands or even coordinating solvent molecules), *via* chemical abstraction assisted by a silver salt, the carbonyl substitution only occurs when electronically excited states are involved (photochemical reaction),[26–28] or when an auxiliary oxidant reagent like trimethylamine-*N*-oxide is employed.[29] This lack of reactivity is attributed to the significant metal-to-carbonyl electron back-donation.[30]

Rhenium(I) complexes containing a monodentate phosphine ligand instead of a halide atom such as the cation *fac*-[(bpy)Re(CO)₃(PR₃)]⁺ have been stated to be selectively photoactive.[26] There are reports of selective replacement of carbonyl ligands in the *trans* position relative to the phosphine ligand, with the release of a molecule of carbon monoxide (CO).[27]

The ability of some molecules to release carbon monoxide (CORMs) under controlled conditions is an interesting property considering the potential therapeutic use of the carbon monoxide against biological targets.[31–34] Many transition metal compounds bearing carbonyl ligands generate carbon monoxide after exposure to light (photoCORMs).[35] Irradiation with enough energy promotes d to π* transitions, thus increasing the oxidation of the metal and consequently weakening its union to the carbonyl.

Rhenium(I) complexes with hybrid P,N-bidentate ligands such as 2-pyridyl-diphenylphosphine (PN) and *N*-(diphenylphosphanyl)pyridin-2-amine (PNN) have been prepared for synthetic or catalytic purposes.[36,37] We have recently reported the synthesis and photophysical properties of facial rhenium(I) tricarbonyl phosphine-imine compounds **RePNBr**, **RePNNBr** and **RePNTfO** (TfO: triflate, Scheme 2).[38–41]
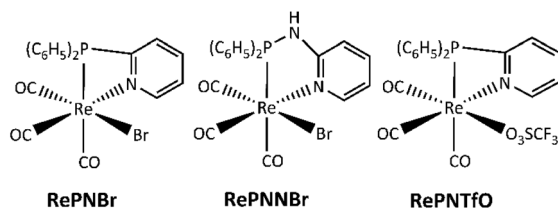
The experimental results indicate that the photophysical properties of these complexes differ from those of their homologs bearing *N,N*-diimine ligands. The former compounds exhibited lower emission quantum yields and shorter luminescence lifetimes, driven by a non-radiative decay process as the main deactivation path, the result of the higher conformational flexibility of the P,N-ligand.[39] Interestingly, these complexes have been found to display dual emission attributed to two emissive MLCT excited states very close in energy: $d\pi \rightarrow \pi^*_{pyridine}$ and $d\pi \rightarrow \pi^*_{phenyl}$.[39] In addition, these three complexes are able to generate singlet oxygen.[39–41]

Recently, the synergic action of singlet oxygen generation and photoinduced release of carbon monoxide by tricarbonyl metal complexes has been proposed as promising treatment against cancer.[42–44] In this framework, rhenium complexes have been classified as good photoCORMs and photosensitizers for singlet oxygen generation, holding also great potential for antibacterial treatments.[45]

Today, there is an urgent need for novel agents to fight bacterial infections. Some standard antibiotics have no action against certain pathogens such as Gram-positive *Staphylococcus aureus* and Gram-negative *Escherichia coli*.[46,47] The overuse and/or misuse of antibiotics has provoked pathogen evolution with higher toughness and novel resistance mechanisms to these antimicrobial agents, posing a tremendous threat to human health,[48,49] increasing the search or development for new treatments like antibacterial photodynamic therapy (aPDT).[50,51]

To the best of our knowledge, no reports are available in the literature about the photochemistry of these or related complexes, despite they offer an opportunity to study the synergic action of singlet oxygen generation and photoinduced release of carbon monoxide in biological systems. Keeping this in mind, we decided to explore the relation between the photochemistry/photophysics of the rhenium complexes **RePNBr**, **RePNNBr** and **RePNTfO** and their antibacterial activity against *S. aureus* and *E. coli*.

Experimental

Reagents and solvents

Compounds **RePNBr** (*fac*-P,N-{(C₆H₅)₂(C₅H₄N)P}Re(CO)₃Br), **RePNNBr** (*fac*-P,N-{(C₆H₅)₂(C₅H₄N)(NH)P}Re(CO)₃Br), and **RePNTfO** (*fac*-P,N-{(C₆H₅)₂(C₅H₄N)P}Re(CO)₃(TfO) where TfO = O₃SCF₃), were synthesized as described in the literature.[38,40,41] All solvents (Merck) were of spectroscopic or HPLC grade. Water was purified and deionized using a Waters Milli-Q system.

Apparatus and procedures

UV-Vis absorption spectra and steady-state kinetic experiments were performed using an Agilent 8453 diode-array spectrophotometer. Rhenium complexes were dissolved in ethanol (EtOH), dichloromethane (DCM) and acetonitrile (MeCN). The photolysis experiments were performed by irradiating 5×10^{-5} M solutions (3 mL) in a 10 mm fluorescence quartz cell, using a Blak-Ray B-100AP high-intensity mercury UV lamp (100 W) with a 365 nm filter at different temperatures (293 K, 303 K and

Scheme 2 Structure of facial rhenium(I) complexes with P,N-bidentate ligands.

313 K). The distance between the quartz cell and the lamp was set at 10.0 cm, with the light source perpendicularly arranged to the sample. The photon flux (I_a) was determined by actinometry using 9,10-dimethylanthracene (DMA) in Freon 113, following the DMA consumption at 334 nm ($I_a = 1.39 \times 10^{-9}$ einstein per s).[52] The kinetic parameters of photolysis were measured by recording the UV-Vis spectra at different irradiation times, using an Agilent 8453 diode-array spectrophotometer. Photolysis experiments followed by infrared measurements were also carried out using a Bruker-Vertex 70 FT-IR instrument.

Assuming a global reaction: $A + I_a \xrightarrow{k_{app}} P$, the apparent kinetic rate constants of the photodegradation process (k_{app}) were obtained following the appearance of the product by monitoring the UV-Vis spectra at different temperatures, and fitting data to eqn (1) (please see ESI† for more details):[53]

$$A_P = \varepsilon_P l [A]_o (1 - e^{-k_{app}t}) \tag{1}$$

where A_P and ε_P correspond to the absorbance and molar extinction coefficient of the product, respectively, l is the optical path and $[A]_o$ represents the initial concentration of the complex. It must be stated that the kinetic rate constants for the photochemical reaction are apparent, as they are dependent on the photon flux and quantum yield of the process,[54,55] however under well-controlled steady-state experimental conditions: irradiation with constant light intensity, geometry unaltered, similar extinction coefficients, these experimental rate constants, denoted as apparent, are fully comparable.

The quantum yields for product formation were calculated using eqn (2):[56]

$$\Phi_P = \frac{\dfrac{d[P]}{dt} V}{I_a} \tag{2}$$

where $d[P]/dt$ is the photoproduct rate formation, V is the solution volume and I_a is the photon flux previously determined by actinometry maintaining the geometry constant.

The activation parameters $\Delta S^{\neq}$ and $\Delta H^{\neq}$ were determined using Eyring eqn (3):[57]

$$\ln\left(\frac{k_{app}}{T}\right) = \ln\left(\frac{k_B}{h}\right) + \frac{\Delta S^{\neq}}{R} - \frac{\Delta H^{\neq}}{R}\frac{1}{T} \tag{3}$$

where k_B, h and R are the Boltzmann constant, Planck constant, and universal gas constant, respectively.

Antibacterial activity

S. aureus (ATCC 29213) and *E. coli* (ATCC 25922) strains were used to assess the antibacterial activity of the studied complexes. Bacteria were cultured in 50 mL flasks containing 10 mL Lysogeny Broth (LB) medium consisting of the following (per liter): 10 g tryptone, 5 g yeast extract, and 0.5 g NaCl. The flasks were placed in a rotary shaking (Orbitron, INFORS) set at 200 rpm and 37 °C for 16 h. Then, the same procedure was repeated as described above and after 5 h of bacterial culture, when the cells were in the middle of the exponential phase, 100 μL of culture were mixed with 700 μL fresh LB medium and 200 μL of complex solutions (initial colony forming units 5×10^5 CFU mL^{-1}) for all the assays. The final established concentrations of the studied compounds were 50 μg mL^{-1} and 300 μg mL^{-1}. Two independent groups of each concentration of rhenium complexes were tested. One group was not irradiated with UV light and the other one irradiated using a Blak-Ray B-100AP high-intensity mercury UV lamp (100 W) with a 365 nm filter for 1 min. Then, the mixture (1 mL of culture) was placed in a 10 mL culture tube and incubated at 37 °C under shaking (200 rpm). After 24 h of culture, the optical density was recorded at 600 nm using a spectrophotometer. Moreover, 100 μL of bacterial suspension was uniformly streaked onto LB agar plates and incubated at 37 °C for 24 h. Finally, the colony forming unit (CFU) was counted for the evaluation of the antimicrobial activity.

Computational details

Geometry optimizations for facial and meridional isomers of **RePNBr** were performed at the B3LYP/6-31+G(d,p) level of theory using the Gaussian 09 Rev C.01 package of programs (G09)[58] starting with **RePNBr** crystallographic coordinates as input.[38] The LANL2DZ basis set was used only for rhenium. Excitations were computed within the time-dependent density functional theory (TD-DFT) methodology, as implemented in G09. Absorption spectra were simulated from the above-mentioned calculations using the GaussSum 3.0 suite of freely available processing tools. A full width at half maximum (FWHM) of the Gaussian curves corresponding to 2500 cm^{-1} was employed to convolute the spectra.

Results and discussion

Photophysical properties

The facial rhenium tricarbonyl complexes bearing P,N-bidentate ligands, namely, **RePNBr**, **RePNTfO**, and **RePNNBr** (Scheme 2), have been characterized in previous works and their main photophysical properties are summarized in Table 1.[39–41] Briefly, they present absorption bands around 315 nm with shoulders at 350 nm, the last, assigned to a metal-to-ligand

Table 1 Summary of the main photophysical properties of the complexes in DCM at 298 K

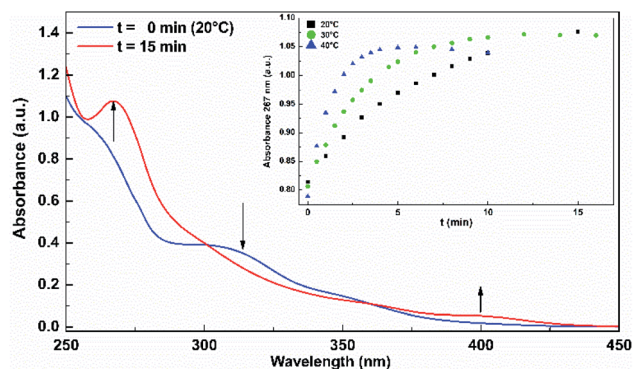| Complex	λ_{abs} (nm)	λ_{em} (nm)	Φ_{em}	τ_{em} (ns)	Φ_Δ	Ref.
RePNBr	315; 355(sh)	550	5.0×10^{-4}	3.8 (87); 39.1 (13)	0.0640	39
RePNTfO	295; 350(sh)	535	1.2×10^{-3}	2.6 (86); 11.6 (14)	0.0200	40
RePNNBr	300; 350(sh)	365	1.3×10^{-2}	2.3 (35); 6.4 (65)	0.0015	41

Fig. 1 Spectral changes of **RePNBr** in EtOH upon irradiation at 365 nm at 20 °C. Inset: increase in absorbance attributed to the product appearance (267 nm) *versus* the irradiation time.

charge transfer (MLCT) transition, which involves π^* orbitals on the pyridine and phenyl rings.

Upon excitation at 350 nm, **RePNBr** and **RePNTfO** exhibit an emission band at around 540 nm with low emission quantum yield, while **RePNNBr** displays an intense emission at 365 nm with an emission quantum yield value of 0.013. This marked difference was attributed to the NH bridge's presence between the phosphorous and the pyridyl group, which modifies the energy levels of the ligand centered (IL) and the MLCT excited states, favoring the emissive path from the IL excited state.[41] The ^{3}MLCT state of all studied complexes is able to photosensitize singlet oxygen through an energy transfer process, with **RePNBr** having the highest value of singlet oxygen quantum yield (Table 1, Φ_Δ). The short lifetimes and low emission quantum yields were attributed to the conformational flexibility conferred by the P,N-ligand, which could favor the non-radiative pathway.

Photochemical behaviour

Irradiation of the complexes in EtOH, DCM or MeCN solutions, at their respective lowest energy absorption bands, gives rise to photoproduct formation. Fig. 1 shows the spectral changes of **RePNBr** in EtOH upon irradiation at 365 nm at 20 °C. As can be observed, the absorption band of **RePNBr** at 315 nm decreases

after irradiation, while two distinguishable bands at 267 nm and 400 nm increase. Similar spectral changes were observed in DCM but less pronounced in MeCN for the three complexes (see ESI†).

The inset in Fig. 1 exhibits an increase in absorbance attributed to the product appearance (267 nm) *versus* the irradiation time. Fitting these data with eqn (1) allows us to obtain the apparent photoproduct formation rate constant (k_{app}). In addition, photodegradation quantum yields (Φ_P) were calculated at room temperature using eqn (2). The values of k_{app} obtained at different temperatures and Φ_P in different solvents are included in Table 2.

The lowest apparent rate constant values and photodegradation quantum yields were observed in MeCN for the three complexes, while the highest ones were found for **RePNBr** in DCM and **RePNTfO** in EtOH. Similar rate constant values arise following the absorbance increase of the photoproduct absorbing at the high energy (267 nm in EtOH) or at the low energy absorption band (400 nm). The photolysis rate constant values were almost not affected by the presence of molecular oxygen, but to discard any other competitive process, all the samples were de-aerated. Besides, the apparent rate constant values increase with the rise in temperature, which is ascribed to a thermal population of the IL excited state from the MLCT excited state with a triplet character.[59] In this context, we apply the transition state theory (Eyring) in order to get information about the transition state.[57]

Fig. 2 presents the Eyring plot for the photolysis of **RePNBr** in different solvents. Fitting the observed photodegradation rate constant values with eqn (2) allows us to get the Eyring parameters summarized in Table 3.

The activation enthalpy ($\Delta H^{\neq}$) values were all positive accompanied by high negative values for the activation entropy ($\Delta S^{\neq}$), being the main contribution to $\Delta G^{\neq}$. This major entropic factor might indicate a more ordered, compact, and probably highly solvated transition state, which is compatible with a reaction occurring through an associative mechanism (I_a).

Mechanism and theoretical calculations

Fig. 3a shows the IR spectral changes of the CO stretching bands after irradiation of **RePNBr** in DCM at room temperature. These changes are compatible with the formation of the *mer*

Table 2 Summary of the apparent photoproduct formation rate constants (k_{app}) and photodegradation quantum yields (Φ_P) for the studied complexes[a]

Solvent	T (K)	RePNBr k_{app} (10^{-3} s^{-1})	Φ_P	RePNNBr k_{app} (10^{-3} s^{-1})	Φ_P	RePNTfO k_{app} (10^{-3} s^{-1})	Φ_P
EtOH	293	2.40	0.155	0.67	0.035	9.91	0.380
	303	5.73		0.78		11.2	
	313	12.3		0.94		12.8	
MeCN	293	0.71	0.165	0.42	0.031	0.49	0.016
	303	1.01		0.45		0.68	
	313	1.55		0.54		0.76	
DCM	293	9.05	0.345	2.07	0.092	2.76	0.191
	303	12.2		2.24		3.60	
	313	15.8		2.48		5.26	

[a] Errors were lower than 10%.

Paper

Fig. 2 Eyring plot for the photolysis of **RePNBr** in different solvents.
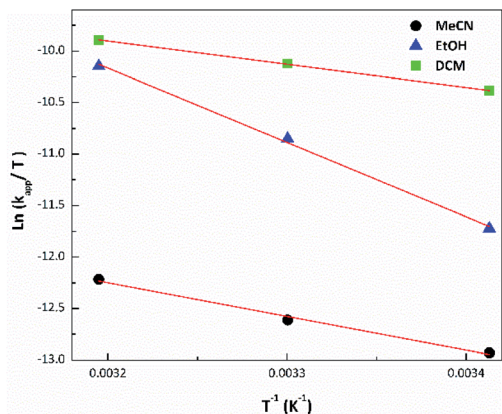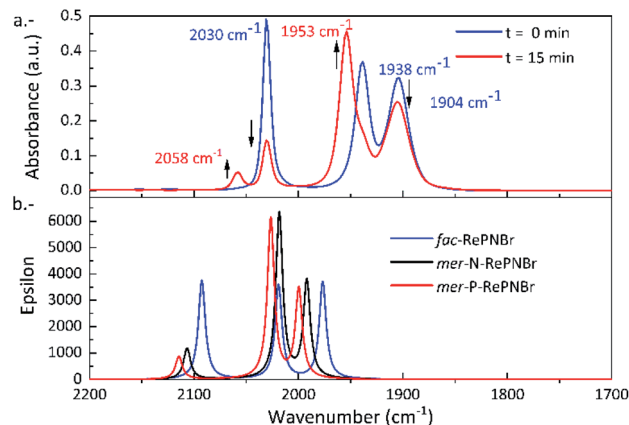

Fig. 3 (a) IR (CO-stretching region) spectra of **RePNBr** in DCM with 0 min (blue) and 15 min (red) of irradiation (365 nm). (b) DFT-computed vibrational spectra for *fac*-**RePNBr** and *mer*-**RePNBr** isomers.

isomer as was reported for other similar complexes.[59] Theoretical calculations support this result, suggesting that isomerization slightly shifts the carbonyl stretching frequencies toward higher energy for the advisable *mer*-isomers (Scheme 3), as shown in Fig. 3b. Indeed, the trans effect of the phosphorous atom would be responsible to address the photoisomerization. Simulation of UV-Vis spectra (Fig. S5†) of each isomer also supports that observed spectral changes are related to an isomerization process, while Fig. S6† shows the DFT-computed vibrational circular dichroism spectra for *fac*-**RePNBr** and its *mer*-isomers.

As commented above, the negative activation entropy change for each complex in each solvent suggests the associative nature of the rate-determining step. We have previously shown that the replacement of triflate by bromide in **RePNTfO** follows this pattern, with a negative activation entropy change of about 60 J K^{-1} mol^{-1}.[40]

Although coincidence, the largely higher negative (around 230 J K^{-1} mol^{-1} in average) values measured for isomerization entropies here are surprising and puzzling. They suggest a rate-determining step where new bonds and/or strong interactions yield an activated complex with less degrees of freedom, and probably also highly constrained in the solvent cage. According to Satos's work,[24] a carbonyl loss reaction begins with an isomerization, involving the formation of penta-coordinate species, which isomerizes and then completes its coordination sphere, or by an associative mechanism, a nucleophilic attack of the solvent could yield to a seven-coordinate intermediate, being the last option the most probable for this particular case. However, Mukuta *et al.*[60] suggested a strong
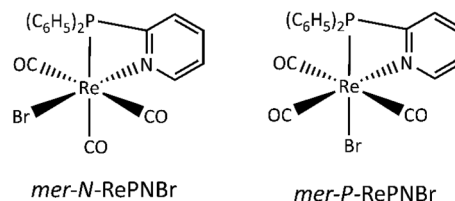
Scheme 3 Possible *mer*-isomers for **RePNBr**.

solvated or even a coordinated solvent molecule-transition state to yield products *via* an associative mechanism. Data presented in Tables 2 and 3 also show that the reactions for **RePNBr** are under each condition significantly faster than that of the analogous complexes **RePNTfO** and **RePNNBr**, and that the coordinating solvents lower the isomerization rate. Finally, no release of carbon monoxide was detected in all the experiments performed.

We have previously shown that chelating 2-pyridylphosphine (PN) may be partially thermally decoordinated from **RePNBr** and replaced with piperidine, leaving [P-{(C$_6$H$_5$)$_2$(C$_5$H$_5$N)P}(C$_5$H$_{11}$N)Re(CO)$_3$Br].[61] Taking account of all these experimental facts, we can propose that the reaction proceeds according the mechanistic sequence shown in Scheme 4.

The excitation of **RePNBr** by UV-Vis leads to an electronic redistribution from the metal to the ligand pyridyl group. One may speculate that this excited molecule would evolve to a highly solvated species, where some lengthening of the

Table 3 Summary of the activation thermodynamic parameters for the photolysis of the studied complexes

Solvent	RePNBr		RePNTfO		RePNNBr	
	$\Delta H^{\ddagger}$ (kJ mol^{-1})	$\Delta S^{\ddagger}$ (J mol^{-1} K^{-1})	$\Delta H^{\ddagger}$ (kJ mol^{-1})	$\Delta S^{\ddagger}$ (J mol^{-1} K^{-1})	$\Delta H^{\ddagger}$ (kJ mol^{-1})	$\Delta S^{\ddagger}$ (J mol^{-1} K^{-1})
EtOH	60.0	−90.0	3.39	−258.4	25.2	−269.8
MeCN	27.2	−212.3	14.2	−259.2	4.27	−288.1
DCM	18.7	−219.9	31.6	−218.8	8.45	−281.5
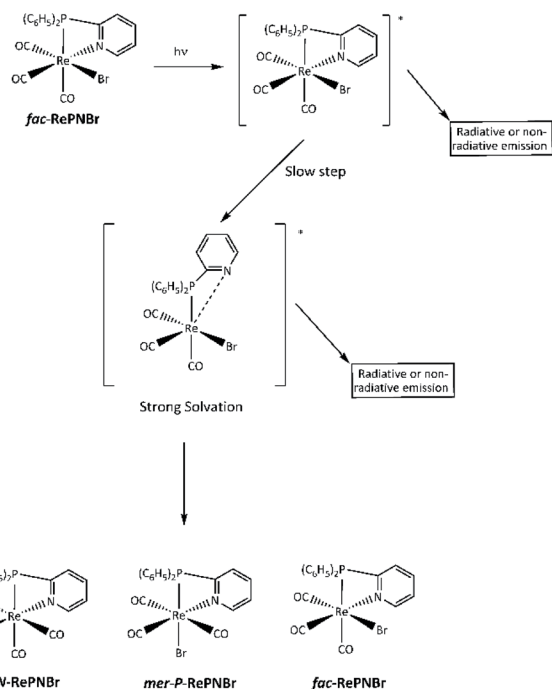
Scheme 4 Proposed isomerization scheme for **RePNBr** photolysis.

rhenium to nitrogen bond occurs. This partially de-coordinated species would quickly isomerize to the *mer*-isomer or re-coordinate the pyridyl arm if radiative emission occurs. The higher reactivity of **RePNBr** compared to **RePNTfO** can be attributed to the presence of the bromide ligand instance to the triflate group, which would facilitate the isomerization due to a trans effect that has also been observed for halide ligands.[28] In addition, the shorter bit of the P,N-ligand in the case of **RePNBr** compared to **RePNNBr** would be the reason for its faster isomerization.

In vitro antibacterial activity

We then assessed the inhibitory effect of **RePNBr**, **RePNTfO**, and **RePNNBr** against two clinically important strains of bacteria, namely, *E. coli* and *S. aureus*. As displayed in Fig. 4A and B, the compounds without irradiation did not arrest *E. coli* growth significantly compared to microbial cultures without adding the complex chemicals. Conversely, *S. aureus* had a 90% decrease in cell viability when exposed to 300 μg mL^{-1} of **RePNTfO** and **RePNBr** (Fig. 4C). By irradiating the complexes with UV light for 1 min and further mixing it with the cell culture, **RePNBr** was the most efficient compound at inhibiting cell propagation for both bacterial strains (99,9%, Fig. 4A and C), independently of the used concentration. *E. coli* was less sensitive to 50 μg mL^{-1} of **RePNTfO** than *S. aureus*. The **RePNNBr** complex provoked cell arrest only against the Gram-negative bacteria *E. coli* employing 300 μg mL^{-1} of the irradiated chemical.

Despite the multiple mechanisms displayed by Gram-positive and -negative bacteria to overcome oxidative stress, namely, the expression of superoxide dismutase, catalases, and peroxidases,[62] or increased levels of glutathione and
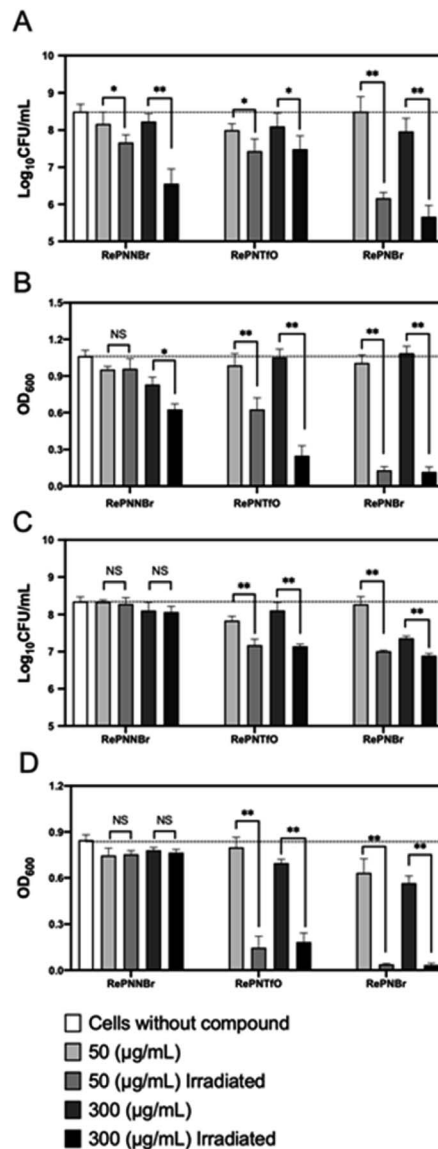

Fig. 4 *In vitro* antibacterial activity of the complexes against *E. coli* and *S. aureus* at 37 °C after 24 h of cultivation. An initial culture of 5×10^5 CFU mL^{-1} was used. (A) *E. coli* cell growth (log$_{10}$ CFU mL^{-1} *versus* rhenium complexes). (B) *E. coli* growth using optical density (OD$_{600}$) determination. (C) *S. aureus* cell growth (log$_{10}$ CFU mL^{-1} *versus* rhenium complexes). (D) *S. aureus* growth using optical density (OD$_{600}$) determination. Mean values and standard deviations were obtained from three independent experiments. NS not significant, *$p < 0.01$, **$p < 0.001$.

carotenoids, the results indicate that the pronounced reduction in cell viability—a 100-fold decrease in the log$_{10}$ CFU value[63]—correlates properly with their singlet oxygen generation capacities, following the same decreasing order **RePNBr** > **RePNTfO** > **RePNNBr**.

Singlet oxygen being highly reactive with any oxidizable cellular compound, it alters cell functioning and facilitates Fe–S release from proteins inactivating their catalytic capacity and altering gene regulation. Besides, the liberated Fe–S species undergoes Fenton chemistry by reacting with H$_2$O$_2$, generating

hydroxyl radicals (OH˙) within the cells and reacting virtually with any macromolecule (DNA, amino acids, RNA, proteins).[64] Herein, we demonstrate that neither *E. coli* nor *S. aureus* can cope with the cascade of oxidative stresses provoked by the generated singlet oxygen from **RePNBr** and **RePNTfO**, making these compounds promising antibacterial agents.

Conclusions

The facial rhenium tricarbonyl complexes bearing P,N-bidentate ligands **RePNBr**, **RePNTfO**, and **RePNNBr** exhibited photoisomerization upon irradiation at 365 nm. The reaction occurs from an intraligand excited state, which is thermally populated from the metal-to-ligand charge transfer (^{3}MLCT) excited state with triplet character. The apparent photo-degradation rate constants depend on the coordinative properties of the solvent, with the lowest values being observed in acetonitrile. Fitting the measured photodegradation rate constants at different temperatures to the Eyring equation allows us to get the activation thermodynamic parameters of the transition state. Positive activation enthalpies ($\Delta H^{\neq}$) accompanied by high negative values for the activation entropy ($\Delta S^{\neq}$) were determined. This result suggests a strongly solvated or compact transition state which is compatible with an associative mechanism for the isomerization. The higher reactivity of **RePNBr** in comparison to **RePNTfO** and **RePNNBr** is due to the shorter bit of the P,N-ligand and to the bromide presence. As no release of carbon monoxide was detected, the antibacterial activity exhibited by the studied complexes is attributed to their singlet oxygen generation capacities, following the same decreasing order **RePNBr** > **RePNTfO** > **RePNNBr**. Because of this result, these compounds can be promising antibacterial agents.

Conflicts of interest

There are no conflicts to declare.

Acknowledgements

Notes and references

1 A. Kumar, S.-S. Sun and A. J. Lees, in *Photophysics of Organometallics*, ed. A. J. Lees, Springer Berlin Heidelberg, Berlin, Heidelberg, 2010, pp. 37–71, DOI: 10.1007/3418_2009_2.

2 D. Gupta and M. Sathiyendiran, *ChemistrySelect*, 2018, **3**, 7439–7458.

3 D. J. Stufkens and A. Vlček, *Coord. Chem. Rev.*, 1998, **177**, 127–179.

4 D. A. Kurtz, K. R. Brereton, K. P. Ruoff, H. M. Tang, G. A. N. Felton, A. J. M. Miller and J. L. Dempsey, *Inorg. Chem.*, 2018, **57**, 5389–5399.

5 J. Hawecker, J.-M. Lehn and R. Ziessel, *Helv. Chim. Acta*, 1986, **69**, 1990–2012.

6 H. Takeda, M. Ohashi, T. Tani, O. Ishitani and S. Inagaki, *Inorg. Chem.*, 2010, **49**, 4554–4559.

7 H. Takeda and O. Ishitani, *Coord. Chem. Rev.*, 2010, **254**, 346–354.

8 X. Q. Guo, F. N. Castellano, L. Li, H. Szmacinski, J. R. Lakowicz and J. Sipior, *Anal. Biochem.*, 1997, **254**, 179–186.

9 L. Li, F. N. Castellano, I. Gryczynski and J. R. Lakowicz, *Chem. Phys. Lipids*, 1999, **99**, 1–9.

10 S. Hostachy, C. Policar and N. Delsuc, *Coord. Chem. Rev.*, 2017, **351**, 172–188.

11 A. M.-H. Yip and K. K.-W. Lo, *Coord. Chem. Rev.*, 2018, **361**, 138–163.

12 G. M. Hasselmann and G. J. Meyer, *Z. Phys. Chem.*, 1999, **212**, 39–44.

13 I. A. Wright, *Polyhedron*, 2018, **140**, 84–98.

14 A. Leonidova, V. Pierroz, R. Rubbiani, J. Heier, S. Ferrari and G. Gasser, *Dalton Trans.*, 2014, **43**, 4287–4294.

15 L. Sacksteder, A. P. Zipp, E. A. Brown, J. Streich, J. N. Demas and B. A. Degraff, *Inorg. Chem.*, 1990, **29**, 4335–4340.

16 R. M. Leasure, L. Sacksteder, D. Nesselrodt, G. A. Reitz, J. N. Demas and B. A. Degraff, *Inorg. Chem.*, 1991, **30**, 3722–3728.

17 L. Wallace and D. P. Rillema, *Inorg. Chem.*, 1993, **32**, 3836–3843.

18 A. Vlcek, *Ultrafast Excited-State Processes in Re(I) Carbonyl-Diimine Complexes: From Excitation to Photochemistry*, Springer, Berlin/Heidelberg, 2010.

19 A. El Nahhas, C. Consani, A. M. a. Blanco-Rodríguez, K. M. Lancaster, O. Braem, A. Cannizzo, M. Towrie, I. P. Clark, S. Záliš, M. Chergui and A. n. Vlček, *Inorg. Chem.*, 2011, **50**, 2932–2943.

20 A. A. Abdel-Shafi, J. L. Bourdelande and S. S. Ali, *Dalton Trans.*, 2007, 2510–2516, DOI: 10.1039/b705524b.

21 F. Ragone, H. H. Martinez Saavedra, P. M. David Gara, G. T. Ruiz and E. Wolcan, *J. Phys. Chem. A*, 2013, **117**, 4428–4435.

22 E. Wolcan, *Inorg. Chim. Acta*, 2020, **509**, 119650.

23 S. Sato, T. Morimoto and O. Ishitani, *Inorg. Chem.*, 2007, **46**, 9051–9053.

24 S. Sato, Y. Matubara, K. Koike, M. Falkenstrom, T. Katayama, Y. Ishibashi, H. Miyasaka, S. Taniguchi, H. Chosrowjan, N. Mataga, N. Fukazawa, S. Koshihara, K. Onda and O. Ishitani, *Chem.–Eur. J.*, 2012, **18**, 15722–15734.

25 T. L. Easun, J. Jia, J. A. Calladine, D. L. Blackmore, C. S. Stapleton, K. Q. Vuong, N. R. Champness and M. W. George, *Inorg. Chem.*, 2014, **53**, 2606–2612.

26 K. Koike, J. Tanabe, S. Toyama, H. Tsubaki, K. Sakamoto, J. R. Westwell, F. P. A. Johnson, H. Hori, H. Saitoh and O. Ishitani, *Inorg. Chem.*, 2000, **39**, 2777–2783.

27 K. Koike, N. Okoshi, H. Hori, K. Takeuchi, O. Ishitani, H. Tsubaki, I. P. Clark, M. W. George, F. P. A. Johnson and J. J. Turner, *J. Am. Chem. Soc.*, 2002, **124**, 11448–11455.

28 S. Sato, A. Sekine, Y. Ohashi, O. Ishitani, A. M. Blanco-Rodríguez, A. Vlček, T. Unno and K. Koike, *Inorg. Chem.*, 2007, **46**, 3531–3540.

29 D. J. Blumer, K. W. Barnett and T. L. Brown, *J. Organomet. Chem.*, 1979, **173**, 71–76.

30 C. Housecroft, *Inorganic Chemistry*, Prentice Hall, 4th edn, 2012.

31 A. F. Tavares, M. R. Parente, M. C. Justino, M. Oleastro, L. S. Nobre and L. M. Saraiva, *PLoS One*, 2013, **8**, e83157.

32 A. F. N. Tavares, M. Teixeira, C. C. Romao, J. D. Seixas, L. S. Nobre and L. M. Saraiva, *J. Biol. Chem.*, 2011, **286**, 26708–26717.

33 R. Motterlini and L. E. Otterbein, *Nat. Rev. Drug Discovery*, 2010, **9**, 728–743.

34 I. Chakraborty, S. J. Carrington and P. K. Mascharak, *Acc. Chem. Res.*, 2014, **47**, 2603–2611.

35 R. D. Rimmer, A. E. Pierri and P. C. Ford, *Coord. Chem. Rev.*, 2012, **256**, 1509–1519.

36 B. Machura and R. Kruszynski, *Polyhedron*, 2006, **25**, 1985–1993.

37 B. Machura and R. Kruszynski, *J. Mol. Struct.*, 2007, **837**, 92–100.

38 F. Venegas, N. Pizarro and A. Vega, *J. Chil. Chem. Soc.*, 2011, **56**, 823–826.

39 N. Pizarro, M. Duque, E. Chamorro, S. Nonell, J. Manzur, J. R. de la Fuente, G. Günther, M. Cepeda-Plaza and A. Vega, *J. Phys. Chem. A*, 2015, **119**, 3929–3935.

40 G. Prado, M. B. Ibañez, A. Acosta, E. Chamorro, P. Hermosilla-Ibáñez, G. Günther, N. Pizarro and A. Vega, *Polyhedron*, 2017, **137**, 222–230.

41 P. Mella, J. C. Palma, M. Cepeda-Plaza, P. Aguirre, J. Manzur, G. Günther, N. Pizarro and A. Vega, *Polyhedron*, 2016, **111**, 64–70.

42 S. C. Marker, S. N. MacMillan, W. R. Zipfel, Z. Li, P. C. Ford and J. J. Wilson, *Inorg. Chem.*, 2018, **57**, 1311–1331.

43 R. N. Pickens, B. J. Neyhouse, D. T. Reed, S. T. Ashton and J. K. White, *Inorg. Chem.*, 2018, **57**, 11616–11625.

44 L. Wu, X. Cai, H. Zhu, J. Li, D. Shi, D. Su, D. Yue and Z. Gu, *Adv. Funct. Mater.*, 2018, **28**, 1804324.

45 L. C.-C. Lee, K.-K. Leung and K. K.-W. Lo, *Dalton Trans.*, 2017, **46**, 16357–16380.

46 B. A. Raho and B. Abouni, in *The Battle Against Microbial Pathogens: Basic Science, Technological Advances and Educational Programs*, ed. A. Méndez-Vilas, Formatex Research Centre, Spain, 2015, vol. I, pp. 637–648.

47 A. r. f. t. N. System, *Am. J. Infect. Control*, 2004, **32**, 470–485.

48 F. C. Tenover, *Am. J. Med.*, 2006, **119**, S3–S10.

49 M. Baym, L. K. Stone and R. Kishony, *Science*, 2016, **351**, aad3292.

50 Y. Liu, R. Qin, S. A. J. Zaat, E. Breukink and M. Heger, *J. Clin. Transl. Res.*, 2015, **1**, 140–167.

51 F. Cieplik, D. Deng, W. Crielaard, W. Buchalla, E. Hellwig, A. Al-Ahmad and T. Maisch, *Crit. Rev. Microbiol.*, 2018, **44**, 571–589.

52 H. J. Kuhn, S. E. Braslavsky and R. Schmidt, *Pure Appl. Chem.*, 2004, **76**, 2105–2146.

53 M. Hippler, *J. Chem. Educ.*, 2003, **80**, 1074.

54 S. R. Logan, *J. Chem. Educ.*, 1997, **74**, 1303.

55 S. Toby, *J. Chem. Educ.*, 2005, **82**, 37.

56 H. Shaw and S. Toby, *J. Chem. Educ.*, 1966, **43**, 408.

57 S. Glasstone, K. J. Laidler and H. Eyring, *The Theory of Rate Processes*, McGraw-Hill, New York, 1941.

58 M. J. T. Frisch, G. W. Trucks, H. B. Schlegel, G. E. Scuseria, M. A. Robb, J. R. Cheeseman, G. Scalmani, V. Barone, B. Mennucci, G. A. Petersson, H. Nakatsuji and M. Caricato, *et al.*, *Revision D.01*, Gaussian, Inc., Wallingford, CT, 2009.

59 S. Sato and O. Ishitani, *Coord. Chem. Rev.*, 2015, **282–283**, 50–59.

60 T. Mukuta, P. V. Simpson, J. G. Vaughan, B. W. Skelton, S. Stagni, M. Massi, K. Koike, O. Ishitani and K. Onda, *Inorg. Chem.*, 2017, **56**, 3404–3413.

61 F. Palominos, C. Muñoz, P. Oyarzun, M. Saldías and A. Vega, *Acta Crystallogr., Sect. E: Crystallogr. Commun.*, 2019, **75**, 1005–1010.

62 R. Gaupp, N. Ledala and G. Somerville, *Front. Cell. Infect. Microbiol.*, 2012, **2**, 33.

63 M. Tim, *J. Photochem. Photobiol., B*, 2015, **150**, 2–10.

64 S. Jang and J. A. Imlay, *J. Biol. Chem.*, 2007, **282**, 929–937.